Supporting Information, including additional methods, discussion, 3 figures and 4 tables for:

Iron isotope fractionation during Fe(II) oxidation mediated by the oxygen-producing marine cyanobacterium *Synechococcus* PCC 7002

Swanner, E.D.[1*], Bayer, T.[2], Wu, W.[2], Hao, L.[3], Obst, M.[4], Sundman, A.[2], Byrne, J. M.[2], Michel, F. M.[5], Kleinhanns, I. C.[2], Kappler A.[2], and R. Schoenberg[2].

[1]Iowa State University, Department of Geological & Atmospheric Sciences, Ames, IA USA.

[2]University of Tuebingen, Department of Geosciences, Tuebingen, Germany.

[3]State Key Laboratory of Environmental Geochemistry, Institute of Geochemistry, Chinese Academy of Sciences, Lincheng West Road 99, Guiyang 550081, P. R. China.

[4]University of Bayreuth, Bayreuth Center of Ecology and Environmental Research, Bayreuth, Germany.

[5]Department of Geosciences, Virginia Tech, Blacksburg, VA, USA.

*Corresponding author: Iowa State University, Department of Geological & Atmospheric Sciences, 2237 Osborn Drive, 253 Science I, Ames, IA 50011-1027, phone: (515) 294-5826, fax: (515) 294-6049, email: eswanner@iastate.edu

Mineral characterization

Aliquots of a culture of *Synechococcus* PCC 7002 grown in the presence of ca. 5 mM Fe(II) were harvested after complete Fe(II) oxidation. Particle size analysis was determined on the sample, suspended in water, with a Mastersizer 2000 (Malvern Instruments GmbH). Brunauer, Emmett, and Teller (BET) surface area analysis was conducted using a Micromeritics ASAP 2000 BET Analyzer. The original sample suspension from the culture was dried directly in the instrument at 40°C under a vacuum.

For ^{57}Fe Mössbauer spectroscopy, the solid fraction produced when ~40% of the starting Fe(II) concentration had been oxidized by *Synechococcus* PCC 7002 was collected, washed with anoxic ultrapure water and air-dried in an anoxic glovebox. A dry powder of the sample was loaded into a Plexiglas® holder (area 1 cm^2). Approximately 10 mg of sample was mixed with 80 mg glucose monohydrate (Roth, Germany) to produce a homogenous powder, which was loaded into a Plexiglas holder (1 cm^2) that was closed to form a thin disc. The sample was housed in a close-cycle exchange gas cryostat (Janis cryogenics) for Mössbauer spectra collection at 295 K, 77 K and 5 K using a constant acceleration drive system (WissEL) in transmission mode with a ^{57}Co/Rh source. The spectra were calibrated against a 7μm thick α-^{57}Fe foil measured at room temperature. Spectra were analyzed using the Recoil software with the Extended Voigt based fitting (xVBF) routine[1].

The doublet present during ^{57}Fe Mössbauer spectroscopy at room temperature is characteristic of an Fe(III) mineral, and the center shift (CS) and quadrupole

splitting (ΔE_q) measured for the sample closely match that of synthetic ferrihydrite (**Supplementary Table 1**)[2]. The sample had a broadened linewidth (and 0.32 mm/s) in comparison to synthetic ferrihydrite (0.23 mm/s). Low temperature measurements indicate maintenance of a doublet-dominated spectrum at 77 K. At 5K, the sample is dominated by a sextet, however the spectra is fitted by only one sextet with a significantly broader linewidth than minerals produced by photoferrotrophic Fe(II) oxidation[3]. The parameters obtained by fitting the spectrum indicate a very poorly crystalline Fe(III)-mineral phase (**Supplementary Table 2**), which likely corresponds to ferrihydrite or nanogoethite. A decreased blocking temperature and increase in the spectral linewidth of the sample as compared to ferrihydrite indicate lower mineral crystallinity[4]. Previous studies have linked an increase in organic matter during ferrihydrite formation to a decrease in particle crystallinity[5, 6], thus it is likely that the decrease in mineral crystallinity in comparison to synthetic ferrihydrite is due to the presence of EPS associated with the minerals (**Figure 3**).

For synchrotron-based X-ray absorption spectroscopy (XAS), the solid product of complete Fe(II) oxidation by *Synechococcus* PCC 7002 was collected and washed with MP medium that contained no nutrients (no phosphate, nitrate, vitamins, trace elements or bicarbonate), i.e. MP buffer. The wet sample was transported to the beamline, loaded into a Teflon sample, sealed with Kapton tape, and frozen. The sample was loaded into a liquid N_2-cooled cryostat. Iron K-edge spectra were collected at beamline 4-1 at Stanford Synchrotron Radiation Lightsource (SSRL). The ring current was 300-350 mA and the energy was 3 GeV. Fluorescence and

transmission spectra were recorded simultaneously using a 13-element germanium detector and ion chambers, respectively. The beamline was equipped with a double crystal monochromator; Si ([220], Φ=90). A Mn 3 μx filter was used to reduce unwanted elastically and inelastically scattered radiation. Furthermore, higher order harmonics were reduced by detuning the monochromator. Spectra were simultaneously recorded for an iron foil placed between the second and third ion chamber to allow for internal calibration. Six spectra were recorded, inspected for beam damage, dead time corrected, energy calibrated by setting the first inflection point of the iron foil to 7112 eV and averaged using SixPack[7]. No self-absorption was observed when comparing fluorescence and transmission spectra (**Supplementary Figure 3**). The averaged transmission spectrum was used for further data analysis.

The X-ray absorption near edge structure (XANES) region was qualitatively processed using the SixPack software[7]. The extended X-ray absorption fine structure (EXAFS) region was subject to wavelet transform (WT) analysis by means of the Igor Pro script[8]. The subsequent shell-by-shell EXAFS fits were accomplished via the computer code Viper[9] and constrained by the wavelet transform (WT) analysis. Briefly, pre- and post-edge functions were subtracted from the spectra, which were subsequently normalized. A spline function was used to subtract background beyond the absorption edge. The k^3-weighted spectrum was fitted in k-space, (2.80-12 $Å^{-1}$) using theoretical phase and amplitude functions from FEFF calculations[10]. Goethite[11] was used as input structure for the FEFF calculation[10]. The amplitude reduction factor (S_0^2) was set to 0.69. This value was obtained by assuming a CN of 6 for the Fe-O paths in the first shell. The numbers of free variables were restricted by

assuming an identical E_0-shift for all shells, and when available, fixing the Debye-Waller factors (σ^2). Therefore, the number of free variables given by the Nyquist theorem ($N_{max} = 2 \times \Delta k \times \Delta R/\pi$, where Δk is the *k*-range of the EXAFS spectrum and ΔR is the R-range of the Fourier transformed range) was never exceeded.

The first derivative XANES analysis revealed a strong resemblance between the sample and the ferrihydrite and goethite references (**Supplementary Figure 2a**). The main peak around 7125 eV also resembles that of the Fe(III)PO_4 reference, but the lack of the strong peak around 7136 eV, which is present in the Fe(III)PO_4 reference, suggests that the sample is dominated by Fe(III) (oxyhydr)oxides. This conclusion was further strengthened by the WT (**Supplementary Figure 2b**), which was dominated by a characteristic feature at ca. 7 $Å^{-1}$, 2.5 Å, caused by the presence of precipitated Fe(III) (oxyhydr)oxides. The shape of this feature indicates that this sample has a ferrihydrite-like structure, since goethite produces features which are shifted to slightly higher *k*-values[12]. The absence of stronger features at lower *k*-values indicates no or low concentrations of second shell light back scatters such as phosphorus or carbon. However, the washing of the solid product before analysis could have removed any organic or iron species sorbed to minerals or cells (e.g. **Figure 3**), hence the lack of Fe-C interactions in the WT plot. Finally, the EXAFS beat pattern between *k* 5-8 $Å^{-1}$ is characteristic for ferrihydrite (**Supplementary Figure 2c**)[13] and the sample fit well using two Fe-O and two Fe-Fe paths (**Supplementary Figure 2C**, **Supplementary Table 3**). The coordination numbers and bond distances obtained are in agreement with those previously published for ferrihydrite[13].

The peaks in the synchrotron XRD data indicate lepidocrocite and goethite are the more crystalline phases present (**Figure 2a**). These phases are still nanocrystalline based on the peak broadening. The average crystal size was estimated to be 10-12 nm for the (020) and (021) directions for lepidocrocite and the (110) direction for goethite using the Scherrer equation. This is consistent with Mastersizer measurements, which indicate that more than 99 % of particles were less than 1 μm in diameter. The broad underlying diffuse intensity is most likely due to the presence of ferrihdyrite, which is likely 2-line ferrhydrite based on the lack of any discernable diffraction features. The pair distribution function (PDF) is dominated by features associated with the Fe(III) (oxyhydr)oxide constituents in the sample. The first peak at ~2 Å is associated with the Fe-O bond length. The features at ~3 and ~3.5 Å are dominantly Fe-Fe pair correlations. The higher r peaks are complex mixtures of Fe-Fe and Fe-O pair correlations[14]. The 3-component linear combination of ferrihydrite, lepidocrocite and goethite (red spectra in **Figure 2b**) resulted in a reasonable fit to the data (**Supplementary Table 4**). Features in the PDF that were not described by any of the 3 components are likely due to the contributions from the organic carbon fraction (e.g. cells, EPS) and phosphate in the sample.

The minerals were characterized as a poorly crystalline ferrihydrite, as a poorly-ordered ferrihydrite by Mössbauer spectroscopy (**Supplementary Figure 1**) and EXAFS (**Supplementary Figure 2**), and 58% ferrihydrite, plus contributions from goethite (22%) and lepidocrocite (20%) as determined by linear combination fitting of the X-ray PDF (**Figure 2**). Samples were air-dried prior to Mössbauer

spectroscopy, and freeze-dried prior to X-ray scattering, which could have caused some transformation of ferrihydrite to more crystalline phases such as goethite[15], indicating that a poorly-ordered ferrihydrite could have been main phase present during oxidation. The detection of goethite and lepidocrocite by X-ray scattering may also result from enhanced sensitivity of that technique to minor mineral phases relative to Mössbauer Spectroscopy and EXAFS.

The mineralogical analyses were always done on minerals produced in separate incubations from the isotope experiments, and at a higher Fe(II) concentration: 5 mM for mineralogy studies vs. 2 mM for isotopic experiments. The minerals for all types of mineral characterization were collected from the same samples, with the Mössbauer results reflecting mineralogy after partial oxidation, which is analogous to some of the time points in isotopic experiments. Previous work in similar types of medium with Fe(II)-oxidizing microbes identified the same minerals within this same range of Fe(II) concentrations (from 2-12 mM). For instance, ferrihydrite was identified as the product of Fe(II) oxidation by the freshwater photoferrotroph *R. ferroooxidans* sp. strain SW2 and the marine photoferrotroph *Rhodovulum iodosum* at 2 mM dissolved Fe(II)[16]. Ferrihydrite was also identified as the product of Fe(II) oxidation at 5 mM Fe(II) for the freshwater photoferrotrophs *R. ferroooxidans* sp. strain SW2, the *Thiodyctyon* strain F4, and *Chlorobium ferrooxidans* strain KoFox[17]. Another example is the identification of goethite as the product of oxidation of 6-12 mM Fe(II) by the nitrate-dependent Fe(II) oxidizing strain *Acidovorax* BoFeN1[18], as well as at 2 mM dissolved Fe(II)[19]. For these reasons we suggest our mineral

characterization at 5 mM Fe(II) are representative of mineralogy in the isotope experiments.

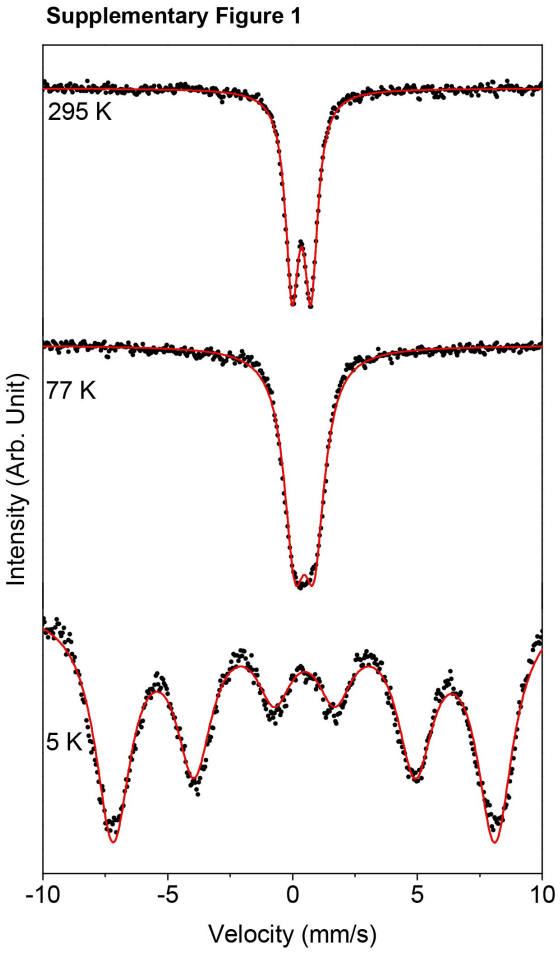

Supplementary Figure 1. ^{57}Fe Mössbauer spectra collected on the sample from *Synechococcus* PCC 7002 at 295, 77, and 5 K. Red lines are fits of the data.

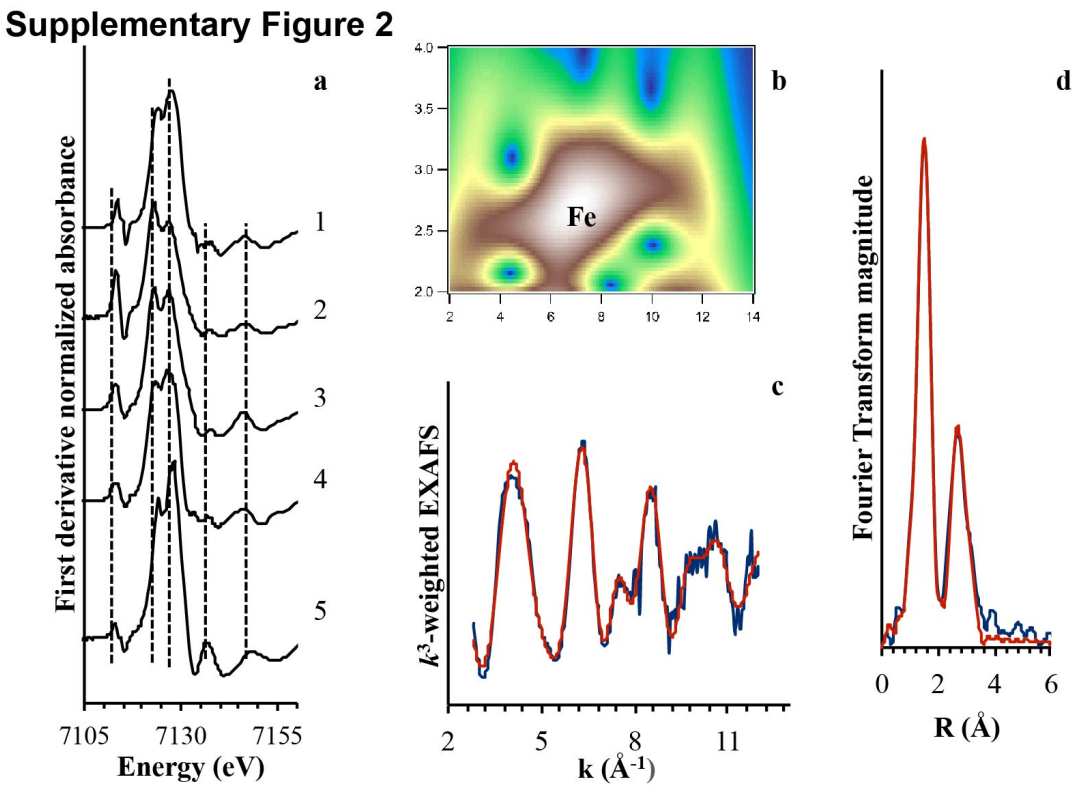

Supplementary Figure 2. a. First derivative Fe K-edge XANES spectra for 1) the solid product after complete Fe(II) oxidation by *Synechococcus* PCC 7002, 2) ferrihydrite with 50 µM Si (Swanner, 2015), 3) 6-line ferrihydrite (Karlsson & Persson, 2012), 4) goethite (Karlsson & Persson, 2012), 5) Fe(III)PO_4 (O'Day, 2004). b. High resolution Fe WT modulus of second and third coordination shells (η=4, σ=2) of the sample. The x-axis is k (2-14 Å^{-1}) and the y-axis is R (2-4Å). c. k^3-weighted and d. Fourier Transformed Fe-EXAFS for the solid sample. The dashed lines are for visual guidance. Blue lines correspond to experimental data and red lines to model data.

Supplementary Figure 3

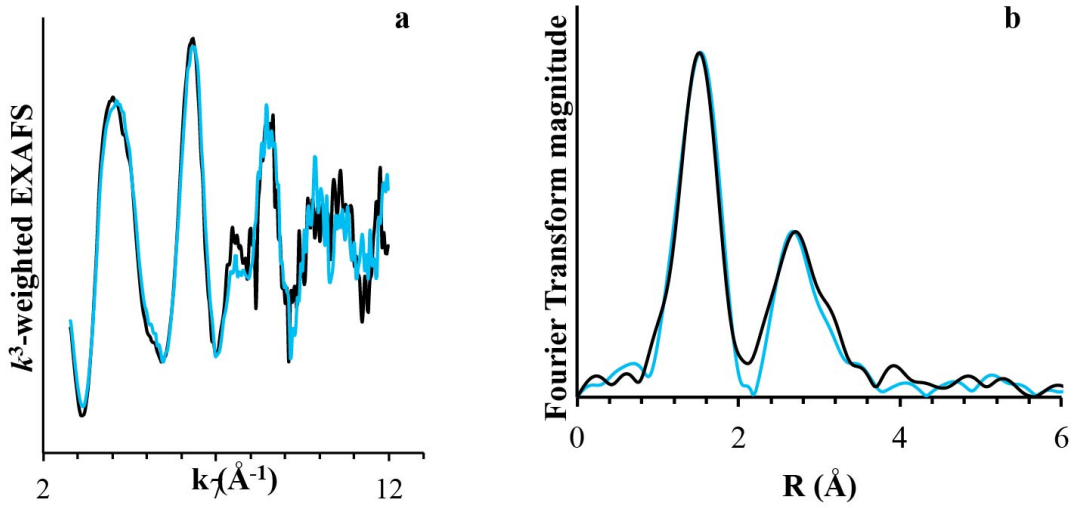

Supplementary Figure 3. a) k^3-weighted and b) Fourier transformed iron EXAFS spectra of the solid product from complete Fe(II) oxidation by *Synechococcus* PCC 7002. Black lines represent transmission data and blue lines represent fluorescence data.

Supplementary Table 1. Fe(II) and Fe(total) concentrations for each of the fractions separated in each replicate. Measurements were made using the Ferrozine assay. One standard deviation (SD) of triplicated measurements (analytical error) is reported. Fe(III) was calculated as the difference between Fe(total) and Fe(II).

Date	Experiment	Sample	Hours	Frac. Fe(II) oxidized	Fe Fraction	Fe(II) (mM)	1SD	Fe(total) (mM)	1SD	Fe(III) (mM)	Recovery (%)
4/1/15	*Sample 1*	A1	0	0	aq	2.12	0.00	1.97	0.00	BD	108
					ppt	BD		ND		ND	
					NaAc	BD		ND		ND	
		B1	7.5	0.42	aq	1.22	0.00	1.14	0.00	BD	78
					ppt	0.02	0.00	0.02	0.00	BD	
					NaAc	0.11	0.00	0.38	0.02	0.28	
		D1	24	0.36	aq	1.36	0.01	1.27	0.00	BD	93
					ppt	0.03	0.01	0.40	0.01	0.37	
					NaAc	0.15	0.00	0.16	0.00	ND	
		E1	44	0.43	aq	1.20	0.00	1.10	0.01	BD	91
					ppt	0.04	0.00	0.50	0.00	0.46	
					NaAc	0.18	0.00	0.20	0.00	0.02	
		F1	68	0.49	aq	1.08	0.01	0.98	0.01	BD	91
					ppt	0.03	0.00	0.63	0.02	0.60	
					NaAc	0.15	0.00	0.17	0.00	0.02	
		G1	92	0.57	aq	0.91	0.00	0.90	0.01	BD	84
					ppt	0.04	0.00	0.56	0.01	0.53	
					NaAc	0.15	0.00	0.19	0.01	0.04	
		H1	116	0.60	aq	0.84	0.00	0.78	0.00	BD	93
					ppt	0.04	0.00	0.85	0.03	0.81	
					NaAc	0.17	0.00	0.21	0.01	0.04	
		I1	140	0.72	aq	0.6	0.02	0.55	0.01	BD	70
					ppt	0.03	0.00	0.64	0.03	0.61	
					NaAc	0.16	0.00	0.19	0.00	0.03	
		J1	188	0.81	aq	0.40	0.00	0.37	0.00	BD	114
					ppt	0.08	0.00	1.65	0.01	1.57	
					NaAc	0.16	0.00	0.22	0.00	0.06	
		K1	260	1.00	aq	BD	0.00	0.00	0.00	BD	116
					ppt	0.08	0.00	2.13	0.01	2.05	
					NaAc	0.04	0.00	0.16	0.01	0.12	
4/1/15	*Sample 2*	A2	0	0.00	aq	2.23	0.01	2.07	0.00	BD	108
					ppt	BD		ND		ND	
					NaAc	BD		ND		ND	
		B2	7.5	0.47	aq	1.19	0.00	1.26	0.05	0.07	79
					ppt	0.02	0.00	0.02	0.00	BD	
					NaAc	0.15	0.00	0.36	0.00	0.24	

D2	24	0.41	aq	1.31	0.02	1.26	0.00	BD	89
			ppt	0.03	0.00	0.41	0.02	0.38	
			NaAc	0.18	0.00	0.17	0.01	BD	
E2	44	0.48	aq	1.17	0.04	1.12	0.01	BD	93
			ppt	0.04	0.02	0.61	0.01	0.57	
			NaAc	0.17	0.00	0.20	0.00	0.02	
G2	92	0.57	aq	0.97	0.00	0.96	0.00	BD	88
			ppt	0.04	0.02	0.65	0.02	0.60	
			NaAc	0.17	0.01	0.22	0.01	0.05	
H2	116	0.56	aq	0.98	0.00	0.92	0.00	BD	91
			ppt	0.03	0.00	0.57	0.01	0.54	
			NaAc	0.38	0.19	0.39	0.00	0.01	
I2	140	0.65	aq	0.78	0.00	0.74	0.01	BD	73
			ppt	0.03	0.00	0.58	0.01	0.55	
			NaAc	0.17	0.00	0.19	0.01	0.02	
J2	188	0.63	aq	0.83	0.00	0.74	0.00	BD	86
			ppt	0.05	0.00	0.83	0.00	0.78	
			NaAc	0.15	0.00	0.20	0.00	0.05	
K2	260	1.00	aq	0.01	0.00	0.00	0.00	BD	106
			ppt	0.06	0.00	1.96	0.07	1.90	
			NaAc	0.05	0.00	0.23	0.00	0.18	

BD = Iron concentrations were below the detection limit of our method (0.01 mM). ND = Iron concentration was not determined for this fraction.

Supplementary Table 2. ^{57}Fe Mössbauer fitting parameters at different temperatures for ferrihydrite and Fe_{ppt} produced by *Synechococcus* PCC 7002. CS – center shift, ΔE_q = quadrupole splitting, H – magnetic hyperfine field, w- linewidth Pop. – relative population.

Sample	Temp. K		CS (mm/s)	±	ΔEq (mm/s)	±	H (T)	±	w (mm/s)	±	Pop. %	±
Ferrihydrite	295	D	0.35	*0*	0.7	*0*			0.23	*0*	100	
Sample	295	D	0.36	*0.01*	0.75	*0.01*			0.32	*0.01*	100	
	77	D	0.47	*0.01*	0.78	*0.01*			0.51	*0.01*	100	
	5	S	0.47	*0.01*	-0.03	*0.02*	47.5	*0.1*	0.87	*0.02*	100	

Supplementary Table 3. k^3-weighted Fe K-edge fit results of the solid product from Fe(II) oxidation by Synechococcus PCC7002.

Path	CN	R (Å)	σ^2 (Å^2)	ΔE_0[a]
Fe-O	2.9	1.95	0.0041	-1.06
Fe-O	3.2	2.06	0.0121	-1.06
Fe-Fe	2.2	3.04	0.0100[b]	-1.06
Fe-Fe	1.4	3.41	0.0100[b]	-1.06

[a] ΔE_0 was assumed to be identical for all shells.

[b] Fixed according to Maillot F., Morin G., Wang Y., Bonnin D., Ildefonse P., Chaneac C., Calas G. (2011) New insight into the structure of nanocrystalline ferrihydrite: EXAFS evidence for tetrahedrally coordinated iron (III). Geochim. Cosmochim. Acta. 75, 2708-2720.

Supplementary Table 4. Linear combination fit (LCF) of the PDF.

Phase	LCF Concentration	% Abundance (normalized)
2-line ferrihydrite	0.3574	58
Goethite	0.1327	22
Lepidocrocite	0.1216	20

Supplementary References

1. Rancourt, D. G.; Ping, J. Y., Voigt-based methods for arbitrary-shape static hyperfine parameter distributions in Mössbauer spectroscopy. *Nuclear Instruments and Methods in Physics Research Section B Beam Interactions with Materials and Atoms* **1991,** *58*, (1), 85-97.
2. Murad, E., Mössbauer spectroscopy of clays, soils and their mineral constituents. *Clay Minerals* **2010,** *45*, (4), 413-430.
3. Swanner, E. D.; Wu, W.; Schoenberg, R.; Byrne, J.; Michel, F. M.; Pan, Y.; Kappler, A., Fractionation of Fe isotopes during Fe(II) oxidation by a marine photoferrotroph is controlled by the formation of organic Fe-complexes and colloidal Fe fractions. *Geochimica et Cosmochimica Acta* **2015,** *165*, (0), 44-61.
4. van der Zee, C.; Roberts, D. R.; Rancourt, D. G.; Slomp, C. P., Nanogoethite is the dominant reactive oxyhydroxide phase in lake and marine sediments. *Geology* **2003,** *31*, (11), 993-996.
5. Eusterhues, K.; Wagner, F. E.; Häusler, W.; Hanzlik, M.; Knicker, H.; Totsche, K. U.; Kögel-Knabner, I.; Schwertmann, U., Characterization of Ferrihydrite-Soil Organic Matter Coprecipitates by X-ray Diffraction and Mössbauer Spectroscopy. *Environ. Sci. Technol.* **2008,** *42*, (21), 7891-7897.
6. Schwertmann, U.; Wagner, F.; Knicker, H., Ferrihydrite–Humic Associations. *Soil Sci. Soc. Am. J.* **2005,** *69*, (4), 1009-1015.
7. Webb, S. M., SIXpack: a graphical user interface for XAS analysis using IFEFFIT. *Physica Scripta* **2005,** *2005*, (T115), 1011.
8. Funke, H.; Scheinost, A. C.; Chukalina, M., Wavelet analysis of extended x-ray absorption fine structure data. *Phys. Rev. B* **2005,** *71*, 1-7.
9. Klementiev, K. V., VIPER for Windows, freeware; K.V. Klementev. *Journal of Physics D: Applied Physics* **2001,** *34*, 209-217.
10. Zabinsky, S. I.; Rehr, J. J.; Ankudinov, A.; Albers, R. C.; Eller, M. J., Multiple scattering calculations of X-ray absorption spectra. *Phys. Rev. B* **1995,** *52*, 2995-30.
11. Szytula, A.; Burewicz, A.; Dimitrijević, Ž.; Kraśnicki, S.; Rżany, H.; Todorović, J.; Wanic, A.; Wolski, W., Neutron diffraction studies of α-FeOOH. . *Phys Status solidi (b)* **1968,** *26*, 429-434.

12. Karlsson, T.; Persson, P., Complexes with aquatic organic matter suppress hydrolysis and precipitation of Fe(III). *Chemical Geology* **2012,** *322-323*, 19-27.
13. O'Day, P. A.; Rivera Jr., N.; Root, R.; Carroll, S. A., X-ray absorption spectroscopic study of Fe reference compounds for the analysis of natural sediments. *American Mineralogist* **2004,** *89*, 572-585.
14. Michel, F. M.; Barrón, V.; Torrent, J.; Morales, M. P.; Serna, C. J.; Boily, J.-F.; Liu, Q.; Ambrosini, A.; Cismasu, A. C.; Brown, G. E., Ordered ferrimagnetic form of ferrihydrite reveals links among structure, composition, and magnetism. *Proceedings of the National Academy of Sciences* **2010,** *107*, (7), 2787-2792.
15. Rapin, F.; Tessier, A.; Campbell, P. G. C.; Carignan, R., Potential artifacts in the determination of metal partitioning in sediments by a sequential extraction procedure. *Environmental Science & Technology* **1986,** *20*, (8), 836-840.
16. Eickhoff, M.; Obst, M.; Schröder, C.; Hitchcock, A. P.; Tyliszczak, T.; Martinez, R. E.; Robbins, L. J.; Konhauser, K. O.; Kappler, A., Nickel partitioning in biogenic and abiogenic ferrihydrite: The influence of silica and implications for ancient environments. *Geochimica et Cosmochimica Acta* **2014,** *140*, 65-79.
17. Kappler, A.; Newman, D. K., Formation of Fe(III)-minerals by Fe(II)-oxidizing photoautotrophic bacteria. *Geochimica et Cosmochimica Acta* **2004,** *68*, (6), 1217-1226.
18. Hohmann, C.; Winkler, E.; Morin, G.; Kappler, A., Anaerobic Fe(II)-oxidizing bacteria show As resistance and co-precipitate As during Fe(III) mineral precipitation. *Environmental Science & Technology* **2010,** *44*, 94-101.
19. Kappler, A.; Schink, B.; Newman, D. K., Fe(III) mineral formation and cell encrustation by the nitrate-dependent Fe(II)-oxidizer strain BoFeN1. *Geobiology* **2005,** *3*, (4), 235-245.